axioms

MDPI

Article

RETRACTED: Diabetic Retinopathy Progression Prediction Using a Deep Learning Model

Hanan A. Hosni Mahmoud

Department of Computer Sciences, College of Computer and Information Sciences, Princ[illegible]Nourah bint Abdulrahman University, P.O. Box 84428, Riyadh 11671, Saudi Arabia; hahosni[illegible].edu.sa

Abstract: Diabetes is an illness that happens with a high level of glucose in the body, and can harm the retina, causing permanent loss vision or diabetic retinopathy. The [illegible]ndus oculi method comprises detecting the eyes to perform a pathology test. In this research, we implement a method to predict the progress of diabetic retinopathy. There is a research gap that exists for the detection of diabetic retinopathy progression employing deep learning models. Therefore, in this research, we introduce a recurrent CNN (R-CNN) model to detect upcoming visual field inspections to predict diabetic retinopathy progression. A benchmark dataset of 7000 eyes from healthy and diabetic retinopathy progress cases over the years are utilized in this research. Approximately 80% of ocular cases from the dataset is utilized for the training stage, 10% of cases are used for validation, and 10% are used for testing. Six successive visual field tests are used as input and the seventh test is compared with the output of the R-CNN. The precision of the R-CNN is compared with the regression model and the Hidden Markov (HMM) method. The average prediction precision of the R-CNN is considerably greater than both regression and HMM. For pointwise classification, R-CNN depicts the least classification mean square error among the compared models in most of the tests. Also, R-CNN is found to be the minimum model affected by the deterioration of reliability and diabetic retinopathy severity. Correctly predicting a progressive visual field test with the R-CNN model can aid physicians in making decisions concerning diabetic retinopathy.

Keywords: deep learning architecture; retinopathy; diabetic retinopathy progression

MSC: 97N

Citation: Hosni Mahmoud, H.A. RETRACTED: Diabetic Retinopathy Progression Prediction Using a Deep Learning Model. *Axioms* **2022**, *11*, 614. https://doi.org/10.3390/axioms11110614

Academic Editors: Jingbo Xia, Tianyong Hao, Qingcai Chen and Hongfei Lin

Received: 9 October 202[illegible]
Accepted: 1 Novem[illegible]r 2022
Published: 4 No[illegible]mber 2022
Retracted: 25 Ma[illegible]2024

1. [illegible]roduction

[illegible] of the main causes of blindness in the world, diabetic retinopathy is defined by the permanent loss of retinal ganglion cells (RGCs) [1,2]. The vision field gradually deteriorates due to structural abnormalities in the RGCs and the optic nerve head [2]. The evaluation and forecasting of the progressive visual field are thought to be crucial processes for maintaining visual function. However, because to the various random mistakes and fluctuations they contain, visual field tests are prone to unpredictability. Clinical knowledge of the evolution of the visual field is hindered by this variability, which is more noticed in ocular cases with diabetic retinopathy than in normal ocular cases [3].

The past several years have seen a lot of interest in and success with studies on machine learning algorithms used to gauge the course of diabetic retinopathy. Visual field defects are divided into 16 archetypes and their evolution is described by the authors in [4]. They used 12,217 eyes from 7360 cases with several reliable 24-2 visual field recording over 5 years. They achieved 90% accuracy in the ground truth validation of 412 eyes with 29.3% confirmed progression. Variation Bayes Linear Regression (VBLR), a sort of machine learning technique, is applied by the authors in [5], and they showed better prediction than pointwise Linear Regression. Deep learning algorithms have recently been used with great success on a variety of tasks as artificial intelligence has advanced. However, only a few

This paper has been retracted. A retraction notice was published on 25 March 2024 in *Axioms* **2024**, *13*, 215. https://doi.org/10.3390/axioms13040215

studies have attempted to use deep learning algorithms to detect visual field progression. A single visual field test is used as the input by the authors in [6] to train a convolutional neural network (CNN) to predict progressive visual fields. Measurements from successive 28-2 visual fields from the years 1998 to 2018 were selected from a public medical database. K-fold cross validation testing with a held out test set was utilized. The model was trained on temporal visual field tests to produce the following predictions for using only a single visual field with accuracy of 90.5%. The authors of [7] presented an auto-encoder trained from low-dimensional standard visual fields utilizing 29,161 fields from 3900 cases. The auto-encoder was trained on a 90% of the dataset of random cases. The remaining 10% was used for the progression of testing. The accuracy is about 90% but with higher CPU time.

Applications involving sequential time series and temporal dependencies have been carried out using recurrent neural networks (RNNs), which are artificial convolutional networks with recurrent connections [8–10]. These have been used successfully for many years in various tasks involving sequence modeling. An RNN can analyze recent data using historical data. Using the dependencies between sequence elements, RNNs are effective predictors [11–13]. The Hidden Markov Model (HMM) and gated recurrent CNN (R-CNN), the two primary RNN variations, attempt to model long-term reliance in lengthy sequences. In contrast to conventional least squares linear regression, HMM has shown a greater ability to predict progressive visual fields according to our prior research. According to the authors in [14], HMM networks could over time detect both local and global patterns in visual fields.

However, the R-CNN performs as well as the HMM and deploys gating units more effectively than a standard HMM [14–18]. Studies in a variety of fields have shown that the R-CNN performs exceptionally well in sequential data analysis when compared to other RNN types [19–22]. RNN has recently been upgraded to a bidirectional technique by simultaneously training in positive and negative time directions, which improves context understanding [23]. Bidirectional gated recurrent CNN (R-CNN) can more accurately forecast visual field advancement, since visual field tests are sequential data with many connections between them. Table 1. depicts recent research in diabetic retinopathy prediction intelligent models.

Table 1. Recent research in diabetic retinopathy prediction intelligent models.

Reference	Research Description	Proposed Solution	Database	Average Accuracy
[24]	Deep learning CNN for early detection of stages of diabetic retinopathy	The model uses markers for classification to predict abnormalities by computing features correlation.	980 Fundus oculi images	91.5%
[25]	Deep learning diagnosis of pre-parametric retinopathy due to diabetes with automated perimetry methodology	Deep learning using Fourier polynomials	Small-sized dataset, cannot be generalized	91.7%
[26]	Cornea classification by mapping visual field of diabetic retinopathy eyes	Pixel-differentiation of the Fundus oculi images	200 Fundus oculi images	91.2% with high recall
[27]	Fundus oculi imaging irregularities detection of optical identification of PCB using transfer learning	Intelligent classification model	unknown	91.7%
[28]	Multi-label retinopathy ocular classification of diabetic macular ischemia utilizing 3-D coherence method	Dense neural network	1300	92.5%
[29]	Quantifying diabetic retinopathy niches using OCT imaging defining DcardNet: multi—classification at multiple levels based on structural and angiographic of optical retinopathy.	Discrete domain-optical analysis	Fundus oculi image 2100 Fundus oculi images	87.93%

Table 1. *Cont.*

Reference	Research Description	Proposed Solution	Database	Average Accuracy
[30]	Deep image CNN for diabetic retinopathy diagnosis.	Feature data mining detection in retinal fundus	950 Fundus oculi images of five labelled diabetic retinopathy cases	89.16%
[31]	Automated cornea image analysis with the exclusion of areas that does not indicate dangerous disease	Regional CNN	4130 Fundus oculi images	90.97%
[32]	Progression diabetic retinopathy in real fundus oculi videos using the fractal dimension	Image-Net convolutional neural network	1700 videos with 25 frames each	88.4%
[33]	Deep learning prediction of proliferative diabetic retinopathy employing optical angiography vascular density	Geometric parameters	1320 3-D Fundus oculi images	90.7%
	Our proposed model	A multitasking fusion deep CNN for detecting the progression of diabetic retinopathy phases from no-diabetic retinopathy to severe diabetic retinopathy progression over 4.3 years on average.	14,000 oculi images	MSE and *p*-values are used

In this paper, we propose a deep learning R-CNN to classify progressive visual field impairment. In this research, we introduce an RNN model and perform performance evaluation and compare the results with regression and HMM models.

The key contribution of this research is to realize higher accuracy by extracting temporal features related to the progress of diabetic retinopathy over 4.3 years on average. The proposed research introduces novel visual field features. Clinical temporal markers of ocular cases are captured from seven successive visual field tests. Temporal features are represented by the input channel to the deep CNN. The dataset is fed to three models, namely: regression, HMM, and R-CNN. A comparison of the three models is performed. The contributions of the proposed research are as follows:

1. The temporal representations of the ocular cases are taken in seven successive visual field tests over 4.3 years to test the progression of the disease and predict the progression using deep learning.
2. The overall accuracy is improved compared to the related work.

The paper is organized as follows: Section 2 describes the materials and methods. Section 3 depicts experimental settings and results. The paper is concluded in Section 4.

2. Dataset

This retroactive research is performed on public datasets of diabetic retinopathy images. The ocular image dataset utilized in this research is gathered from a public diabetic retinopathy database. The progress of diabetic retinopathy is depicted in Figure 1.

Ocular cases are taken from seven successive visual field tests that are utilized in the training and validation datasets. There is no overlap between the training and validation datasets. Eyes with intermission of 4 years between the first and seventh visual field tests are included. For instance, if there are thirteen successive visual field tests, the first to sixth tests are used as the initial data and the seventh to the test number 12 are used as the subsequent data. The test number 13 is omitted from the database. The tests numbered 6 and 12 are employed in the prediction phase, and the left behind tests are employed in the training as depicted in Figure 2.

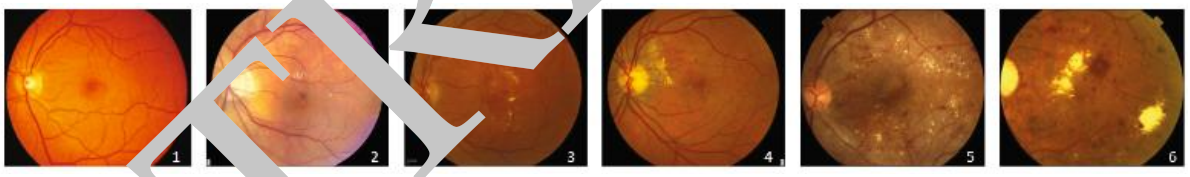

Figure 1. The progress of diabetic retinopathy with image 1 from a mild to a severe case in image 6.

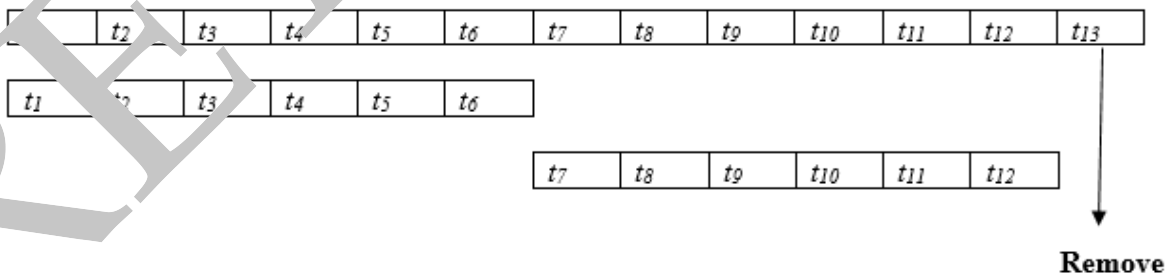

Figure 2. The timeline of the images of a patient who went through thirteen visual field tests. The visual field test times are specified in the timeline and are utilized in training, and those in the black timeline are utilized in the prediction.

2.1. Random Errors and Fluctuations to Visual Field Tests

Visual field tests of the public dataset are done employing the 28–2 modeling with the Swedish Threshold model on a Field Analyzer III (Karl Xeiss Meditec, Inc., San Francisco, CA, USA). Visual fields are tested for fluctuations and errors comprising eyelid artifacts,

lack of attention or tiredness effects. We also omitted artifacts such as faulty fixation or evidence of glaucoma, which can affect the results; any tests with such artifacts were excluded from this study. Visual fields can be unreliable and the loss function can exceeds 35% of errors in false negative rate.

We obtained 8323 visual field data consisting of 6-cells from 6685 eyes of 4593 ocular cases. Datasets from 7051 (85%) and 1272 (15%) are used as the training and test sets, respectively. A total of 7051 records from the training dataset are randomly split to training and validation datasets at a ratio of 9:1. The validation data are used to prevent overfitting through checking the current fitness of the neural network during training. All 8323 datasets had exactly six visual field tests, and the average follow-up period for each of the six visual field tests is 4.39 ± 1.69 years. Table 2 shows the information for each dataset.

2.2. Training and Testing Dataset

Diabetic retinopathy cases are classified into five classes: normal, mild diabetic retinopathy, moderate diabetic retinopathy, severe diabetic retinopathy and proliferative diabetic retinopathy as depicted in Table 3. Mild diabetic retinopathy begins with minute alterations in blood vessels, and recovery can still be achieved at this stage. If the patient has not received treatment, the case will progress to moderate diabetic retinopathy accompanied with blood vessel leakage. The diabetic retinopathy will then progress to severe and proliferative cases and may lead to vision impairment [34–36].

To classify diabetic retinopathy with better precision using a deep learning model, a large size dataset is required for training. Table 4 depicts more information on the count of images in each diabetic retinopathy class in both the training and testing subsets.

Table 2. Characteristics of the datasets.

Characteristics	The Whole Dataset	Training Data	Testing Data
Number of ocular cases (each eye)	14,000 (7000)	11,200 (5600)	2800 (1400)
Age; average ± standard deviation	49.96 ±16.04	44.11 ±14.88	49.19 ±16.84
Initial field: IF (dB); average ± standard deviation	−4.89 ±6.21	−4.77 ±6.16	−6.19 ±6.44
Follow up (years); average ± standard deviation	4.69 ±2.74	4.87 ±2.87	4.61 ±1.84
Average number of visual field tests	8.48 ±2.08	8.82 ±2.22	6.00 ±0.00
IF ≥ -6 dB	4416	2688	828
-5 dB $>$ IF ≥ -13 dB	1218	881	226
-13 dB $>$ IF	1062	846	208
Dataset extension			
Cases of the dataset with eight eyes series	8222	8061	1282
Follow up (years); average ± standard deviation	4.28 ±1.68	4.26 ±1.66	4.61 ±1.84
Duration time (years); average ± standard deviation	0.84 ±0.82	0.82 ±0.81	1.00 ±0.84
IF ≥ -5 dB	6688	4861	828
-5 dB $>$ IF ≥ -13 dB	1488	1241	226
-13 dB $<$ IF	1268	1068	208

Table 3. Classes of diabetic retinopathy.

Progress in Years	0	2–4 Years	4–8 Years	8–12 Years	>12 Years
Class of diabetic retinopathy	Normal	Mild diabetic retinopathy	Moderate diabetic retinopathy	Severe diabetic retinopathy	Proliferate diabetic retinopathy
Damage to retina	No retinopathy	Minute alteration in blood vessels.	blood vessels leakage.	Larger blood leakages and. vessel blockage.	Vision loss.

Table 4. The count of images in each diabetic retinopathy classes.

Diabetic Retinopathy Class/Count of Images	Training Set		Testing Set	
	Left Eye	Right Eye	Left Eye	Right Eye
Normal (No diabetic retinopathy)	1224	122[illegible]	[illegible]7	203
Mild diabetic retinopathy	1200	[illegible]1	19[illegible]	189
Moderate diabetic retinopathy	2102	224[illegible]	395	390
Severe diabetic retinopathy	421	448	313	318
Proliferate diabetic retinopathy	35[illegible]	355	305	300

2.3. Visual Field Test

Automated primary tests are [illegible]ne using a Hu[illegible]phrey Visual device 750i (Carl Zeiss Meditec, Boston, MA, USA) with th[illegible]reshold [illegible]gorithm (ITA) 28-2 or 34-2. Among the 62 points of the 28-2 te[illegible]rangement, two points of biological scotoma are left out, and the remaining points are u[illegible]lized[illegible] 34-2 test arrangement is transformed to 28-2 utilizing test points. Robust visua[illegible] field [illegible]ests [illegible]epicted as having a false-positive ratio of less than 35%, a false-negative ratio [illegible] less tha[illegible] 35%, and a fixation loss value of less than 35%.

2.4. Co[illegible]volutio[illegible]l Neural Ne[illegible]work

[illegible] used t[illegible]e convolutic[illegible]al neural networks HMM and R-CNN. Python language 3.8 (Google [illegible]., [illegible]Y, USA) was used to classify the visual field test.

A. HMM[illegible]d R-CNN

We constru[illegible]ed a one-layer CNN to train on the structure of the utilized dataset utiliz-[illegible] preprocessed training data. The HMM neural networks are defined in Equations (1)–(5) as [illegible]ows:

$$F_g = \left(S_f I_t + S_{Lf} L_{t-1} + P_f\right) \quad (1)$$

$$I = (S_i I_t + S_{Li} L_{t-1} + P_i) \quad (2)$$

$$O = (S_o I_t + S_{Lo} L_{t-1} + P_o) \quad (3)$$

$$(A)_t = (A)_{t-1} \otimes \left(F_g\right)_t + (I)_t \otimes (\tanh(S_C I_t + S_{LC} L_{t-1}) + P_C) \quad (4)$$

$$L_t = O \otimes \tanh((A)_{t-1}) \quad (5)$$

where, I is the input, O is the output, is the activation function S_f, S_i, S_o, and S_C and P_f, P_i, P_o, and P_C represent the score and preference bias using various steps in the CNN, respectively, of three gates and a RAM cell and $\otimes$ is the dot product of two vectors.

The definitions of the input gate I and output gate O are utilized to regulate the memory flow of inputs and outputs into the remaining part of the CNN, while F_g is an auxiliary to the cells which authorizes the output of more weight values from the prior neuron to the subsequent neuron. The data located in the memory cells is influenced by the greater activation values; if the input has greater activation function value, the data will be stored in the memory. In addition, if the output has greater activation function value, it permits the data to go to the following neuron. If not, the input data with the greater

weight values will be stored in the memory. The sigmoid and tanh are activation functions. L (t − 1) denotes the previous hidden convolutional layer that computes the weights. After computing Equation (4), (A) t turns into the up-to-date memory cell. Equation (5) displays the dot multiplication of the previous hidden layer value and prior cell. The non-linear property of the gates using tanh and sigmoid are produced, which are depicted in Equations (1)–(5) The quantity $t-1$ and t are prior and present time periods.

R-CNN is an alternative of HMM which contains two gates—the update and the reset gates. The R-CNN has no extra memory cell to store the data; hence, it can control the data included in the unit, as depicted in Equations (6)–(9).

$$G_{update} = (S_u I_t + S_{Lu} L_{t-1} + P_u) \quad (6)$$

$$G_{reset} = (S_r I_t + S_{Lr} L_{t-1} + \quad (7)$$

$$\widetilde{L_t} = tanh(SI_t + S(G_{reset} \quad L_{t-1})) \quad (8)$$

$$L_t = \left(1 - \left(G_{update}\right)_t\right) \otimes I \quad + \left(G_{update}\right)_t \otimes \quad (9)$$

The update gate G_{update} in Equation (6) defines the amount of information that has been changed. In Equation (7), the reset gate G_{reset} is comparable to G_{update}; if G_{reset} is reset to zero, it captures the input and overlooks the prior computed state. Furthermore, $\widetilde{L_t}$ denotes the equivalent functionality as in R-CNN, and L_t computes the linear function between the present $\widetilde{L_t}$ and the prior L_{t-1} activation function value in Equations (8) and (9).

A reverse and forward R-CNN is joined to formulate an R-CNN convolutional layer. These layers utilize the same input but will learn differently and join the results to produce the output. Deep neural networks can be effective at mapping activation functions and representing variable dependencies [20–22]. We can establish that R-CNN has higher performance on the datasets.

B. Proposed Model and Experimental Results

In the proposed model, the deep learning includes three phases: feeding the data, the sequential neural network layer that is utilized for predictions, and dense layers. The convolutional neural structures for both HMM and R-CNN are depicted in Figure 3.

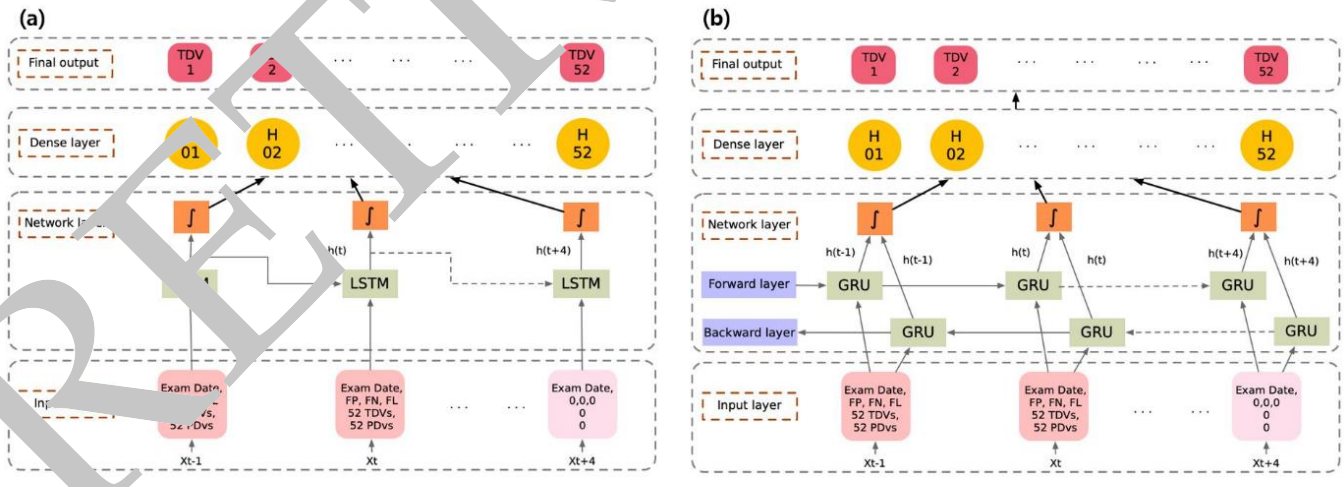

Figure 3. The architecture of the HMM and R-CNN models. HMM = Hidden Markov; R-CNN = recurrent CNN; DV = Deviation value. (**a**) The structure of the HMM method (**b**) The structure of the proposed R-CNN model.

Figure 3a shows the structure of the HMM method. The HMM model has been introduced in [13].

Figure 3b depicts the structure of the proposed R-CNN model. The input layers comprise five successive data values from I_{t-1} to I_{t+3} and the final classification output I_{t+4}, with an output of 60 classes on the final exam.

The sequence diagram of the proposed model is depicted in Figure 4.

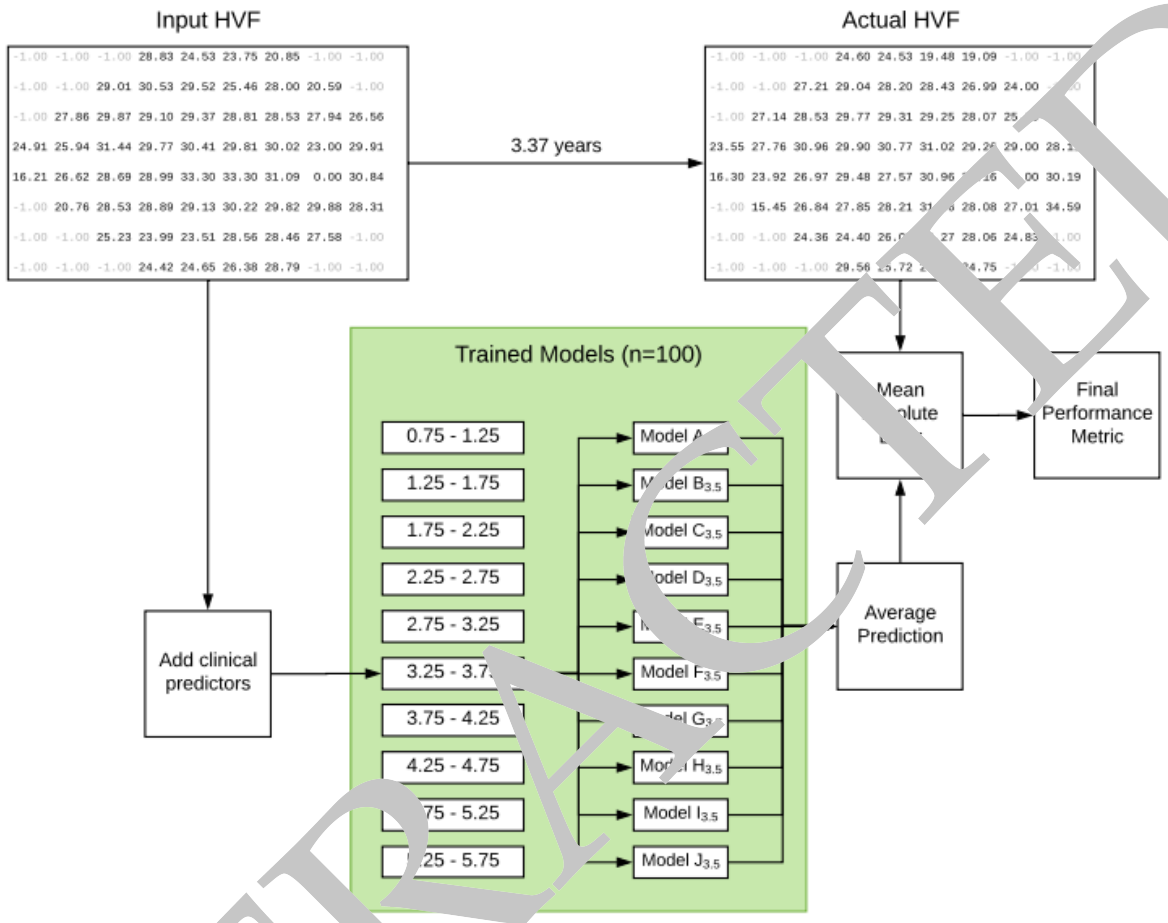

Figure 4. The sequence diagram of the model testing.

The sequential convolutional neural model comprised eight parallel HMM or CNN units. The architecture of the HMM and R-CNN models are presented in Figure 3a,b, respectively.

The initial seven units receives 120 features, including 72 deviation values (DV) and 48 pattern values (PTV). Metrics including false negative, false positive and fixation loss ratios are presented as well as the time metric. To enhance the precision of the deep learning prediction, all of the inputs are divided by the average value and normalized. The DV, PTV, and time metric values are partitioned into 60, 60, and 1100 samples, respectively. The final cell utilizes the normalized time metric value. Later, the convolutional neural layer is linked to the following dense layer with 62 neurons which produce the final output and 62 visual predictions where each neuron produces one visual field value.

3. Experiments

3.1. Experimental Results Analyses

The mean square error (MSE) and mean absolute error (MAE) of the DV are utilized as precision measures. The MSE is computed for left and right eyes as depicted in Equations (10) and (11).

$$MSE = \sqrt{\sum_{n=1}^{52} \frac{(actual\ DV_n - classified\ DV_n)^2}{62}} \quad (10)$$

where, n is the number of the test points of the visual field.

MAE is computed for each test point of the visual field for all eyes using the following Equation:

$$MAE_i = \sum_{i=1}^{n} \frac{|TDV_i - PTDV_i|}{n} \quad (11)$$

where, n is the number of eyes, TDV_i is the actual value and $PTDV_i$ is the predicted case.

A variance analysis is done to evaluate the three models. At the time of rejection of the null hypothesis, the average hypothesis is significant and is adopted, and ad hoc computation is done utilizing a t-test. In all statistical studies, $p < 0.05$ indicates a significant result.

3.2. Experimental Results

Table 2 depicts the demographic statistics of the testing portion of the dataset. The utmost diagnosis is principal open angle diabetic retinopathy (57.28%). The mean classification time (the time slot between classification and the final visual field test) is 1.02 ± 0.74 years, as depicted previously. The mean MSE and points mean absolute error (PMAE) are depicted in Tables 5 and 6.

Table 5. Statistics of the test dataset.

	Number of Cases
Total	2100
Gender: Male	1092 (52%)
Diagnosis	
Diabetic retinopathy suspect	560
Primary open angle diabetic retinopathy	840
Pseudo exfoliation diabetic retinopathy	100
Primary angle closure diabetic retinopathy	299
Secondary diabetic retinopathy	190
Others	111

Table 6. Comparison of average MSE and P-value between regression method, HMM, and R-CNN.

		Regression Method	HMM	R-CNN	ANOVA *p*-Value	*p*-Value		
						Regression Method vs. R-CNN	HMM vs. R-CNN	Regression Method vs. HMM
Prediction error, average ± standard deviation	MSE (dB)	5.81 ±5.89	5.06 ±3.61	5.71 ±3.53	<0.001	<0.001	<0.001	<0.001
	PMAE (dB)	5.53 ±0.56	5.10 ±0.59	3.80 ±0.56	<0.001	<0.001	<0.001	<0.001

Confusion matrices are presented in Tables 7–9 for the regression model, HMM, and the proposed deep learning model for the five classes of diabetic retinopathy.

Table 7. Confusion matrix for the regression model (300 test cases for each class).

		Predicted Cases				Proliferate
		Normal	Mild	Moderate	Severe	
Actual Cases	Normal (No diabetic retinopathy)	280	12	8	0	
	Mild diabetic retinopathy	10	270	15	3	2
	Moderate diabetic retinopathy	1	16	270	0	3
	Severe diabetic retinopathy	0	0	3	290	
	Proliferate diabetic retinopathy	0	0	2	5	273

Table 8. Confusion matrix for the HMM.

		Predicted Cases				Proliferate
		Normal	Mild	Moderate	Severe	
Actual Cases	Normal (No diabetic retinopathy)	285	10	5	0	0
	Mild diabetic retinopathy	10	7	8	3	2
	Moderate diabetic retinopathy	1	14	280	5	0
	Severe diabetic retinopathy	0	0	0	293	7
	Proliferate diabetic retinopathy	0	0	1	19	280

The classification precision of the R-CNN model is higher than the regression and HMM precisions. The mean square error of the R-CNN is 2.91 ± 1.32 dB and the MSEs of the regression and HMM models are 3.71 ± 3.59 dB and 3.06 ± 3.61 dB, respectively. The differences in the classification errors are significant ($F = 45.14$, $p < 0.0015$). The mean square error of the R-CNN is considerably less than the other models (both $p < 0.0015$).

The count of cases discarded by the mean square error classification error is depicted in Figure 5. The varieties where the classification error of R-CNN comprised 50% or more of the total count of cases are ≤3 dB (630 cases, 42.11%) and 3–4 dB (275 cases, 14.16%). The equivalent ranges of the classification mean error by the regression method are ≤3 dB (429 cases, 31.86%) and 3–4 dB (291 cases, 21.97%), and the results of the HMM are ≤3 dB (605 cases, 39.70%) and 3–4 dB (165 cases, 13.97%).

Table 9. Confusion matrix for the R-CNN.

		Predicted Cases				
		Normal	**Mild**	**Moderate**	**Severe**	**Proliferate**
Actual Cases	Normal (No diabetic retinopathy)	292	8	0	0	
	Mild diabetic retinopathy	3	293	4	0	0
	Moderate diabetic retinopathy	0	4	290	[illegible]	1
	Severe diabetic retinopathy	0	0	0	295	
	Proliferate diabetic retinopathy	0	0	[illegible]	[illegible]	295

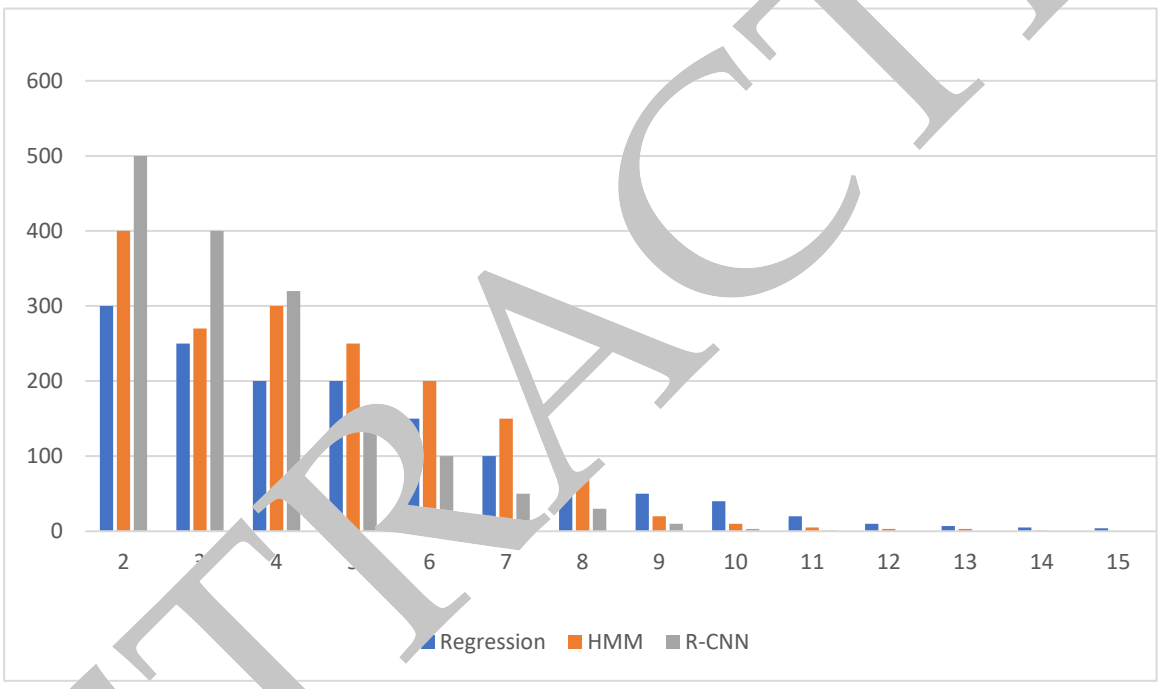

Figure [illegible]he number of cases according to the mean prediction error (DB).

The visual field mean absolute error is depicted in Figure 6. Of the 62 DV points, [illegible]-CNN displayed the least classification error in the different methods. R-CNN displayed considerably higher precision at point 30 (red circles) and point 50 (blue circles) as opposed to the regression and HMM, respectively.

Table 10 depicts the mean square classification error (MSE) for the various field tests, as displayed in Figure 7. The 30–2 field is partitioned into six partitions as presented in [21–23]. The eye optic nerve anatomy (visual and temporal) are utilized. In all partitions, the classification errors of the R-CNN are considerably less than regression and HMM ($p \leq 0.0015$).

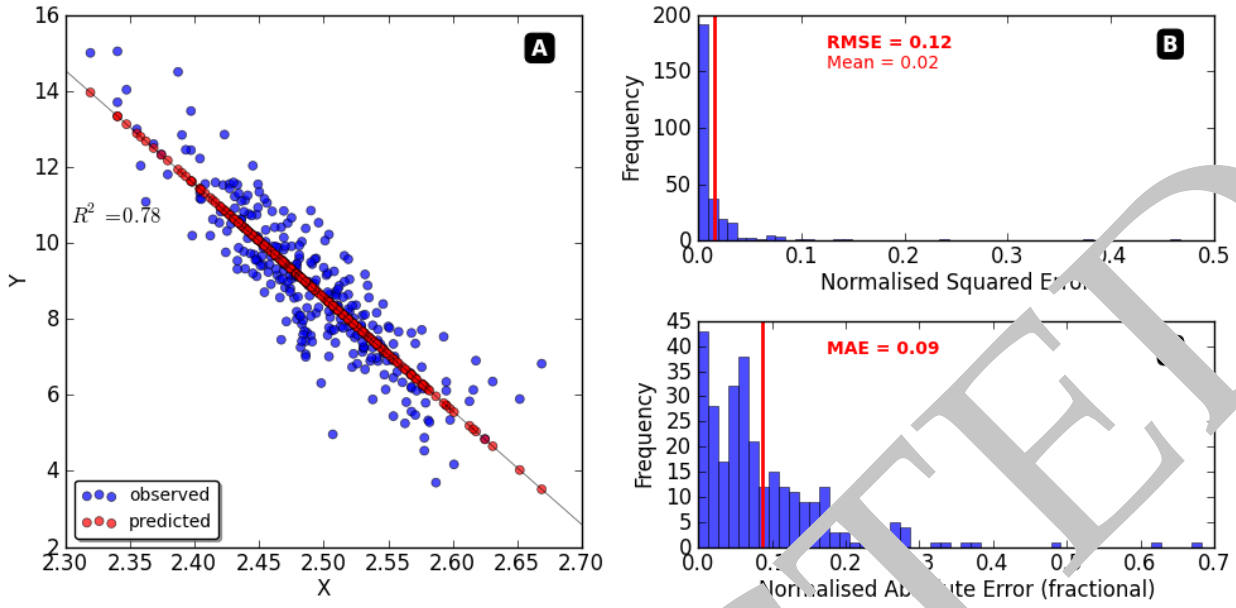

Figure 6. (**A**) Mean absolute error (MAE) of classified deviation value (DV). R-CNN had the least classification error (MAE) in most of the points. The more opaque blue indicates greater error. Red dots depict significant variances between the regression and R-CNN; blue dots depict significant variances between HMM and R-CNN (t-test). (**B**) Normalized squared error (**C**) Normalized absolute error.

Table 10. The prediction error (MSE) by visual field partitions.

	Prediction Error (MSE, dB), Average ± Standard Deviation			*p*-Value		
	Regression Method	HMM	R-CNN	R-CNN vs. HMM	R-CNN vs. Regression Method	Regression Method vs. HMM
Spatial	4.85 ±5.08	4.39 ±3.86	4.02 ± 3.55	<0.001	<0.001	<0.001
Temporal	4.94 ±5.5	4 ±4.53	4.38 ±3.91	<0.001	<0.001	0.310
Intertemporal	5.58 ±.19	4.78 ±.05	4.54 ± 3.85	<0.001	<0.001	<0.001
Nose angle	5.54 ±5.	5.30 ±4.	4.97 ± 4.36	<0.001	<0.001	<0.001
Marginal	5.00 ±4.95	5.05 ±3.60	4.74 ± 3.58	<0.001	<0.001	<0.001
Dominant	5.08 ±5.18	4.76 ±4.15	4.44 ± 3.68	<0.001	0.001	<0.001

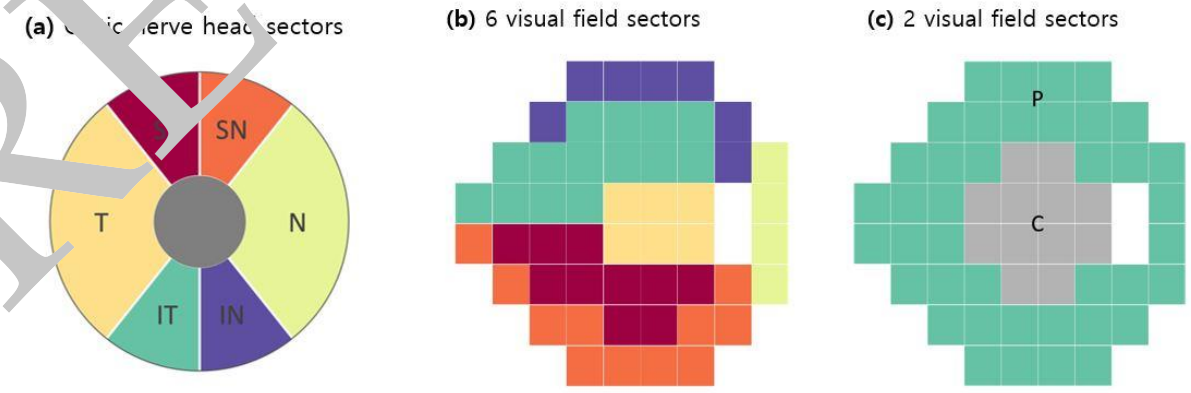

Figure 7. Representation of the optic nerve (**a**) and spatial field (**b**,**c**). (**b**) The spatial field is partitioned into six parts (**c**) The spatial field is partitioned into central and marginal parts.

The mean MSE error discarded by the different parameters are depicted in Table 11 and Figure 8. The classification error of R-CNN is considerably less in cases of false positive, false negative, and loss rate as opposed to the other models ($p \leq 0.028$); as MD increases, the classification errors of all methods decrease.

Table 11. Mean classification error (MSE) according to reliability metrics.

	Prediction error (MSE, dB), Average ± Standard Deviation			**Number of Eyes**	***p*-Value**			
	Regression Method	**HMM**	**R-CNN**		**R-CNN vs. HMM**	**R-CNN vs. Regression Method**	**Regression Method vs. HMM**	**ANOVA**
prediction error vs. false positive rate (FPR, %)								
FP rate ≤ 2	5.90 ± 5.43	5.06 ± 3.65	4.71 ± 3.55	797	<0.001	<0.001	<0.001	<0.001
2 < FP ≤5	5.75 ± 4.35	5.18 ± 3.69	4.80 ± 3.54	358	<0.001	<0.001	<0.001	<0.001
5 < FP ≤8	5.43 ± 3.53	4.83 ± 3.48	4.53 ± 3.18	73	<0.001	<0.001	0.007	<0.001
8 < FP ≤10.0	4.90 ± 3.38	4.74 ± 3.14	4.45 ± 1.95	57	<0.001	0.001	0.431	<0.001
FP rate > 10	5.15 ± 4.19	5.19 ± 3.54	4.85 ± 3.44	88	<0.001	<0.001	<0.001	<0.001
prediction error and false negative (FN rate %)								
FN rate ≤ 2.5	5.34 ± 4.88	4.58 ± 3.59	4.33 ± 3.31	766	<0.001	<0.001	<0.001	<0.001
2 < FN ≤5	5.16 ± 3.93	4.43 ± 1.79	4.10 ± 1.59	155	<0.001	<0.001	<0.001	<0.001
5 < FN ≤8	5.63 ± 4.03	5.05 ± 3.41	5.57 ± [illegible]	109	[illegible]	<0.001	0.007	<0.001
8 < FN ≤ 10.0	5.65 ± 3.91	5.53 ± 3.05	5.30 ± 1.[illegible]9	[illegible]1	<0.001	<0.001	<0.001	<0.001
FN rate > 10	7.43 ± 5.67	6.36 ± 4.04	5.95 ± 4.0[illegible]	151	<0.001	<0.001	<0.001	<0.001
prediction error vs. loss function (L, %)								
L ≤ 3	5.91 ± 5.88	5.04 ± 3.75	[illegible]66 ± 3.53	518	<0.001	<0.001	<0.001	<0.001
3 < L ≤ 5	6.55 ± 3.99	5.[illegible]	3.30 [illegible].17 ± 3.06	14	0.003	0.035	0.533	<0.001
5 < L ≤ 8	5.59 ± 3.87	5.08 ± [illegible]	[illegible]	175	<0.001	<0.001	0.001	<0.001
8 < L ≤ 11	4.95 ± 4.[illegible]	4.05 ± 3.19	3.86 ± 3.10	141	<0.001	<0.001	<0.001	<0.001
L > 11	5.98 ± 3.[illegible]	5.45 ± 3.50	[illegible] ± 3.45	545	<0.001	<0.001	<0.001	<0.001
Classification error and mean deviation (D, dB)								
D < −11	7.[illegible]0 ± 5.56	6.9[illegible] ± 3.59	6.30 ± 3.69	340	<0.001	<0.001	0.174	<0.001
−11 ≤ D < [illegible]8	6.8[illegible] ± 3.86	6.57 ± [illegible]3.05	5.85 ± 3.10	80	<0.001	<0.001	0.339	<0.001
−8 ≤ D < −[illegible]	5.9[illegible] ± 3.55	5.54 ± 1.90	5.03 ± 1.80	153	<0.001	<0.001	0.003	<0.001
−5 < D < −2	[illegible]68 ± 4.97	4.70 ± 1.95	4.55 ± 1.73	378	<0.001	<0.001	<0.001	<0.001
−3 ≤ D	4.[illegible] ± 4.[illegible]3	3.38 ± 1.38	3.15 ± 1.17	553	<0.001	<0.001	<0.001	<0.001

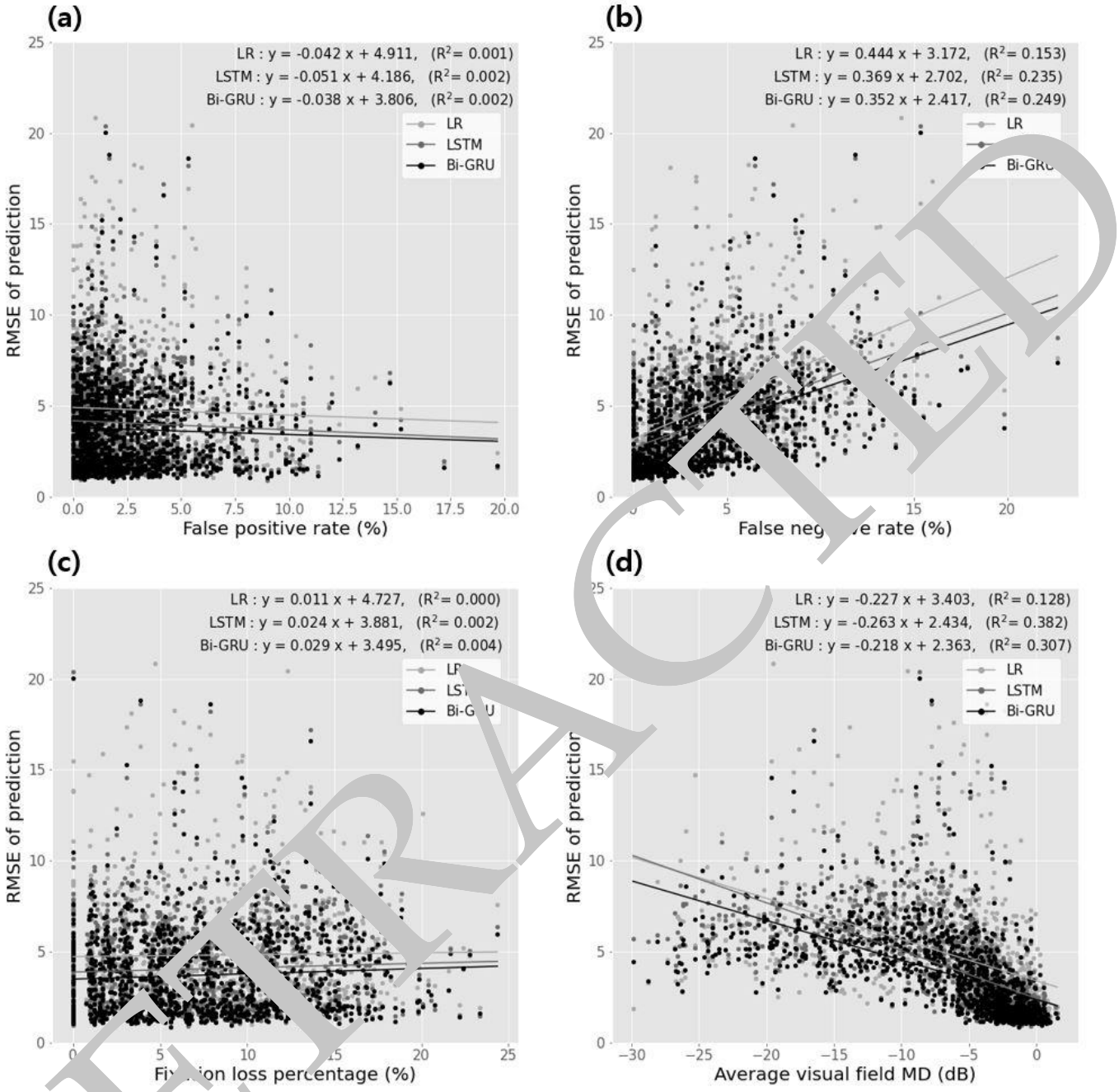

Figure 8. Regression investigation of classification error (MSE) and other parameters. (**a**) MSE correlation with false positive rate. (**b**) MSE correlation with false negative rate. (**c**) MSE correlation with loss function value. (**d**) MSE correlation with visual field mean deviation (D).

The correlation of the classification error and other parameters are depicted in Table 12 and Figure 8. The mean square error increases as the false negative rate increases. In addition, MSE increases as the loss function value increases. MSE decreases as visual field D increases ($p < 0.025$) in all models, as depicted in Figure 8.

Table 12. Correlation coefficients and linear regression analyses between classification error and reliability and between classification error and visual field average deviation.

	Correlation Coefficients		Linear Regression Analysis			
	Spearman's rho	***p*-Value**	**Slope**	**Intercept**	**R^2**	***p*-Value**
classification error vs. false positive rate						
Regression method	−0.024	0.344	−0.042	4.911	0.001	0.329
HMM	−0.043	0.040	−0.041	4.184	0.00[illegible]	0.048
R-CNN	−0.042	0.134	−0.038	3.804	0.[illegible]02	0.141
classification error vs. false negative rate						
regression method	0.444	<0.001	0.444	3.142	0.143	<0.[illegible]1
HMM	0.443	<0.001	0.349	2.40[illegible]	0.[illegible]4	<0.001
R-CNN	0.448	<0.001	0.342	[illegible].414	0.[illegible]	<0.001
classification error vs. fixation loss percentage						
regression method	0.083	0.003	0.011	4.42[illegible]	<0.001	0.424
HMM	0.041	0.029	0.[illegible]24	3.881	0.002	0.101
R-CNN	0.044	0.004	0.029	3.494	0.004	0.032
classification error vs. average visual field average deviation						
regression method	−0.441	<0.001	−0.224	3.4[illegible]3	0.128	<0.001
HMM	−0.443	<0.001	[illegible]243	[illegible].434	0.382	<0.001
R-CNN	−0.444	[illegible].001	−0.2[illegible]	2.343	0.304	<0.001

4. Conclusions

In thi[illegible]search, we [illegible]roposed an intelligent model to predict diabetic retinopathy progres[illegible]ion o[illegible]r the years[illegible]s an auxiliary diagnostic tool. This tool can aid in predicting retin[illegible]pathy pr[illegible]gression at [illegible] early stage and help clinical professionals take fast and efficie[illegible]reatr[illegible]steps.

In t[illegible]esearch, R-CNN displayed a higher classification accuracy than regression and HMM mode[illegible]n all areas of the visual field. Also, the R-CNN network has higher accuracy in the central r[illegible]ns than the other methods. These results are clinically significant due [illegible]the protectio[illegible]n of the central visual area. This protection is important for the quality of li[illegible]alue of the ocular patients with diabetic retinopathy [27–29]. In the present study, R-C[illegible]is the least affected by the worsening of reliability indices. The false negative and fi[illegible]ation losses affected visual field classification among the reliability indices in all models. However, the correlation coefficient of fixation losses is weak, and R2 is also small, [illegible]ndicating that the effect of fixation losses is small. Previous studies reported that false negative rates are associated with visual field assessment, but fixation losses are not. Other studies reported that fixation losses are the most common cause of unreliable visual field classification [32–36].

The limitations of our study include the following: First, there is a lack of generality according to the degree of diabetic retinopathy severity; ocular cases with early diabetic retinopathy with D > −6 dB are included relatively more in the training and test datasets than ocular cases with advanced diabetic retinopathy. This may have affected R-CNN model learning, but it can be more helpful as it reflects the ratio of actual ocular cases in real clinical practice. Second, we did not include clinical data in the training.

For future work, we aim develop a deep learning architecture by adding clinical characteristics to the input data. Comparative time complexity analysis will also be included. In the future we will also create a benchmark dataset for use in experiments. We will employ a preprocessing phase with data augmentation to enhance performance. In addition, a detection technique with bounding boxes can enhance time complexity and precision.

In summary, this study shows that a deep learning architecture utilizing the R-CNN algorithm, a variant of RNN, can predict progressive visual field tests significantly better than the pointwise regression method and HMM algorithms. The R-CNN model is less affected by the reliability indices of the visual field input data. This could aid in decision-making by accurately predicting progressive visual field tests in clinical practice. Our R-CNN algorithm can also help clinicians make treatment decisions for oc[illegible] that have difficulty undergoing repeated visual field tests.

Funding: This research is funded by Princess Nourah bint Abdulrahman [illegible]ersity Researche[illegible] Supporting Project number (PNURSP2022R113), Princess Nourah bin[illegible] Abdul[illegible]man Universi[illegible], Riyadh, Saudi Arabia.

Acknowledgments: I would like to thank Princess Nourah bint A[illegible]dulrahman University [illegible]archers Supporting Project number (PNURSP2022R113), Princess N[illegible]bint A[illegible]dulrahman [illegible]niversity, Riyadh, Saudi Arabia.

Conflicts of Interest: The authors declare no conflict [illegible]nterest.

References

1. Resnikoff, S.; Pascolini, D.; Etya'Ale, D.; Kocur, I.; Pararajasegaram, [illegible]Poknarel, G.P.; [illegible]ariotti, S.P. Global data on visual impairment in the year 2002. *Bull. World Health Organ.* **2004**, *9*, 844–8[illegible]1.
2. Weinreb, R.N.; Aung, T.; Medeiros, F.A. The Pathophysiology an[illegible] Treatment of Diabetic reti[illegible]opathy: A Review. *JAMA* **2014**, *311*, 1901. [CrossRef]
3. Henson, D.B.; Chaudry, S.; Artes, P.H.; Faragher, E.B.; Ansons, A[illegible]esponse Variability [illegible]n the Visual Field: Comparison of Optic Neuritis, Diabetic retinopathy, Ocular Hypertension, and Norma[illegible]ves. *Investig. Opht[illegible]almol. Vis. Sci.* **2000**, *41*, 5.
4. Wang, M.; Shen, L.Q.; Pasquale, L.R.; Petrakos, P.; Formica, S.; Bo[illegible] M.V.; Welli[illegible], S.R.; De Moraes, C.G.; Myers, J.S.; Saeedi, O.; et al. An Artificial Intelligence Approach to Det[illegible]t Visual Field Pro[illegible] Diabetic retinopathy Based on Spatial Pattern Analysis. *Investig. Ophthalmol. Vis. Sci.* **2019**, *60*, 365. [illegible]Ref] [PubMed]
5. Murata, H.; Araie, M.; Asaoka, R. A New Approach t[illegible] Meas[illegible]ual Field Progression in Diabetic retinopathy Ocular cases Using Variational Bayes Linear Regression. *Investig. Op[illegible]thalm[illegible]ol. Vis[illegible]*. **2014**, *55*, 8386–8392. [CrossRef]
6. Wen, J.C.; Lee, C.S.; Keane, P.A.; Xiao, S[illegible] Rokem, A.S.; [illegible]en, P.P.; W[illegible]u, Y.; Lee, A.Y. Forecasting progressive Humphrey Visual Fields using deep learning. *PLoS ON[illegible]* **20[illegible]**[illegible]4, e0214875. [CrossRef] [PubMed]
7. Berchuck, S.I.; Mukherjee, S.; Med[illegible]ros, F.A. [illegible]stimating Ra[illegible]s of Progression and Predicting Progressive Visual Fields in Diabetic retinopathy Using a Deep Varia[illegible]l Autoe[illegible]coder. *Sci. Re[illegible]*. **2019**, *9*, 18113. [CrossRef]
8. Jun, T.J.; Eom, Y.; Kim, D.; Kim, [illegible] Pa[illegible]n, H.M.; Kim, D. TRk-CNN: Transferable ranking-CNN for image classification of glaucoma glaucoma s[illegible]ect, and normal eyes. *Expert Syst. Appl.* **2021**, *182*, 115211. [CrossRef]
9. Manias, G.; Kiourtis, A[illegible] Mavrogiorgou, [illegible] Kyriazis, D. Multilingual Sentiment Analysis on Twitter Data Towards Enhanced Policy Making. In P[illegible]oce[illegible]gs of the IFIP Int[illegible]tional Conference on Artificial Intelligence Applications and Innovations, León, Spain, 14–17 Jun[illegible]2022; Sp[illegible]er: Cham, Swi[illegible]zerland, 2022; pp. 325–337.
10. Kattenborn, T[illegible] Leitloff, J.; Sch[illegible]r, F.; Hinz, S. Review on Convolutional Neural Networks (CNN) in vegetation remote sensing. *ISPRS J. Photogramm. Remote Sens[illegible]* **2021**, *173*, 24–49. [CrossRef]
11. Salehin[illegible]ad, H.; Sankar, S.; Barfe[illegible], J.; Colak, E.; Valaee, S. Recent Advances in Recurrent Neural Networks. *arXiv* **2017**, arXiv[illegible]01078.
12. Liu, S.; Ya[illegible] N[illegible] Li, M.; Zh[illegible]u, M. A Recursive Recurrent Neural Network for Statistical Machine Translation. In Proceedings of the 52nd An[illegible]l Meeting [illegible]the Association for Computational Linguistics, Baltimore, MD, USA, 22–27 June 2014; Volume 1, pp. 14[illegible]1500.
13. You[illegible]g, T.; Hazarik[illegible].; Poria, S.; Cambria, E. Recent Trends in Deep Learning Based Natural Language Processing. *IEEE Comput. Intel[illegible]. Mag.* **2018**, *13*, 55–75. [CrossRef]
14. Hoch[illegible]chmidhuber, J. Long Short-Term Memory. *Neural Comput.* **1997**, *9*, 1735–1780. [CrossRef] [PubMed]
15. [illegible]hung, J.; Gulcehre, C.; Cho, K.; Bengio, Y. Empirical Evaluation of Gated Recurrent Neural Networks on Sequence Modeling. *ar[illegible]* **2014**, arXiv:1412.3555.
16. Park[illegible]; Kim, J.; Lee, J. Visual Field Classification using Recurrent Neural Network. *Sci. Rep.* **2019**, *9*, 8385. [CrossRef]
17. Dixi[illegible], A.; Yohannan, J.; Boland, M.V. Assessing Diabetic retinopathy Progression Using Machine Learning Trained on Longitudinal Visual Field and Clinical Data. *Ophthalmology* **2021**, *128*, 1016–1026. [CrossRef] [PubMed]
18. Lynn, H.M.; Pan, S.B.; Kim, P. A Deep Bidirectional R-CNN Network Model for Biometric Electrocardiogram Classification Based on Recurrent Neural Networks. *IEEE Access.* **2019**, *7*, 145395–145405. [CrossRef]
19. Cho, K.; van Merrienboer, B.; Gulcehre, C.; Bahdanau, D.; Bougares, F.; Schwenk, H.; Bengio, Y. Learning Phrase Representations using RNN Encoder–Decoder for Statistical Machine Translation. *arXiv* **2014**, arXiv:1406.1078.
20. Khandelwal, S.; Lecouteux, B.; Besacier, L. *Comparing R-CNN and Hmm For Automatic Speech Recognition*; LIG: Indore, India, 2016.

21. Li, X.; Li, X.; Ma, X.; Xiao, F.; Xiao, C.; Wang, F.; Zhang, S. Time-series production forecasting method based on the integration of Bidirectional Gated Recurrent CNN (R-CNN) network and Sparrow Search Algorithm (SSA). *J. Pet. Sci. Eng.* **2022**, *208*, 109309. [CrossRef]
22. Darmawahyuni, A.; Nurmaini, S.; Rachmatullah, M.N.; Firdaus, F.; Tutuko, B. Unidirectional-bidirectional recurrent networks for cardiac disorders classification. *Telkomnika* **2021**, *19*, 902. [CrossRef]
23. Schuster, M.; Paliwal, K.K. Bidirectional recurrent neural networks. *IEEE Trans. Signal Process.* **1997**, *45*, 2673–2681. [CrossRef]
24. Ferreira, J.; Júnior, A.A.; Galvão, Y.M.; Barros, P.; Fernandes, S.M.M.; Fernandes, B.J. Performance Improvement of Path Planning algorithms with Deep Learning Encoder Model. In Proceedings of the 2020 Joint IEEE 10th International Conference on Development and Learning and Epigenetic Robotics (ICDL-EpiRob), Valparaiso, Chile, 26–30 October 2020; pp. 1–6.
25. Pascanu, R.; Gulcehre, C.; Cho, K.; Bengio, Y. How to Construct Deep Recurrent Neural Networks. *arXiv* 2013, arXiv:1312.6026.
26. Gomes, J.C.; Masood, A.I.; Silva, L.H.d.S.; da Cruz Ferreira, J.R.B.; Júnior, A.A.F.; dos Santos Rocha, A.L.; de Oliveira, L.C.P.; da Silva, N.R.C.; Fernandes, B.J.T.; Dos Santos, W.P. COVID-19 diagnosis by combining RT-PCR and pseudo-convolutional machines to characterize virus sequences. *Sci. Rep.* **2021**, *11*, 1–28.
27. Majumder, S.; Elloumi, Y.; Akil, M.; Kachouri, R.; Kehtarnavaz, N. A deep learning-based smartphone app for real-time detection of five stages of diabetic retinopathy. In *Real-Time Image Processing and Deep Learning 2020*; International Society for Optics and Photonics; SPIE: Bellingham, WA, USA, 2020; Volume 11401, p. 1140106.
28. Asaoka, R.; Murata, H.; Iise, A.; Araie, M. Detecting Preperimetric Diabetic retinopathy with Standard Automated Perimetry Using a Deep Learning Classifier. *Ophthalmology* **2016**, *123*, 1974–1980. [CrossRef] [PubMed]
29. Garway-Heath, D.F.; Poinoosawmy, D.; Fitzke, F.W.; Hitchings, R.A. Mapping the Visual Field to the Optic Disc in Normal Tension Diabetic retinopathy Eyes. *Ophthalmology* **2000**, *107*, 7.
30. Silva, L.H.d.S.; George, O.d.A.; Fernandes, B.J.; Bezerra, B.L.; Lima, E.B.; Oliveira, S.C. Automatic Optical Inspection for Defective PCB Detection Using Transfer Learning. In Proceedings of the 2019 IEEE Latin American Conference on Computational Intelligence (LA-CCI), Guayaquil, Ecuador, 11–15 November 2019; pp. 1–6.
31. Borrelli, E.; Sacconi, R.; Querques, L.; Battista, M.; Bandello, F.; Querques, G. Quantification of diabetic macular ischemia using novel three-dimensional optical coherence tomography angiography metrics. *J. Biophotonics* **2020**, *13*, e202000152. [CrossRef]
32. Zang, P.; Gao, L.; Hormel, T.T.; Wang, J.; You, Q.; Hwang, T.S.; Jia, Y. DcardNet: Diabetic retinopathy classification at multiple levels based on structural and angiographic optical coherence tomography. *IEEE Trans. Biomed. Eng.* **2020**, *68*, 1859–1870. [CrossRef]
33. Ayala, A.; Ortiz Figueroa, T.; Fernandes, B.; Cruz, F. Diabetic Retinopathy Improved Detection Using Deep Learning. *Appl. Sci.* **2021**, *11*, 11970. [CrossRef]
34. Dai, L.; Wu, L.; Li, H.; Cai, C.; Wu, Q.; Kong, H.; Liu, R.; Wang, X.; Hou, X.; Liu, Y.; et al. A deep learning system for detecting diabetic retinopathy across the disease spectrum. *Nat. Commun.* **2021**, *12*, 3242. [CrossRef]
35. Lyu, X.; Jajal, P.; Tahir, M.Z.; Zhang, S. Fractal dimension of retinal vasculature as an image quality metric for automated fundus image analysis systems. *Sci. Rep.* **2022**, *12*, 1–868. [CrossRef]
36. Pour, E.K.; Rezaee, K.; Azimi, H.; Mirbagheri, B.; Fadakar, K.; Faghihi, H.; Mirshahi, A.; Ghassemi, F.; Ebrahimiadib, N.; et al. Automated machine learning based classification of proliferative and non-proliferative diabetic retinopathy using optical coherence tomography angiography vascular density maps. *Graefes Arch. Clin. Exp. Ophthalmol.* **2022**. [CrossRef]